Title

A Comprehensive Comparison of the Phase Change Material-Based Internal and External Cooling Systems

Journal

ECS Transactions, 97(7)

ISSN

1938-5862

ISBN

9781607688952

Authors

Zhao, Rui
Liu, Jie
Ma, Fai

Publication Date

2020-06-25

DOI

10.1149/09707.0195ecst

Peer reviewed

ECS Transactions, 97 (7) 195-206 (2020)
10.1149/09707.0195ecst ©The Electrochemical Society

A Comprehensive Comparison of the Phase Change Material-Based Internal and External Cooling Systems

Rui Zhao[a], Jie Liu[b] and Fai Ma[a]

[a] Department of Mechanical Engineering, University of California, Berkeley, CA 94720, USA
[b] Department of Mechanical and Aerospace Engineering, Carleton University, Ottawa, ON K1S 5B6, Canada

In this study, phase change material (PCM) is used internally and externally in managing the heat generation of cylindrical Li-ion batteries during high rate discharges. Both internal and external cooling systems are thoroughly compared in their cooling effect on batteries of different sizes (18650, 21700, and 26650) and radial thermal conductivities, their cooling effect on battery packs of different layers (2, 4, and 8 layers of batteries), the necessity using high thermally conductive PCM in the cooling systems, as well as their weight and volume added to the battery system. Results show that the internal cooling system is more suitable for high specific energy applications. It is less sensitive to the battery radial thermal conductivity and performs better for large battery packs and thick batteries. While the external cooling system is more space-saving and suitable for 2-layer battery packs with forced convection applied at the battery pack side walls. However, its performance deteriorates as the thermal conductivity of PCM and batteries decreases.

Introduction

Being employed in a wide range of energy storage applications, such as solar energy storage systems and electric vehicles (EVs), lithium-ion (Li-ion) batteries have become an important link in the chain of clean energy harvest and delivery and have played a crucial role in low-carbon energy transitions. Thermal management is critical for maintaining the efficiency, safety, and longevity of LIBs due to the exothermic behavior and high temperature sensitivity of LIBs [1]. A desirable thermal management system should be able to help sustain a desired operating temperature range and a small temperature gradient within batteries.

Having a jelly-roll or stacked structure, Li-ion batteries have a much lower thermal conductivity in the series direction than the parallel direction because the separators hinder the heat transfer. As a result, the temperature difference developed inside the battery is of a great concern especially for thick batteries. Cylindrical batteries usually have a lower specific surface area compare to pouch and prismatic batteries, and larger cylindrical batteries have become more and more popular due to the reduced cost. The heat transfer in the radial direction, therefore, is of particular importance to be investigated. For example, the heat accumulation effect in the center of cylindrical LIBs has been observed and experimentally studied by Shah *et al.* [2] and Zhang *et al.* [3]. The insufficient cooling in the battery center can cause temperature nonuniformity and lead to battery performance

degradations in long-term operation. Meanwhile, the temperature uniformity of batteries is highly dependent on the radial thermal conductivity, as a consequence, a few research works have experimentally investigated the radial thermal conductivity of cylindrical batteries, and different results were obtained. For example, Bhundiya *et al*. measured a radial thermal conductivity of 0.2 W m^{-1} K^{-1} in a 22650 battery [4], while a radial thermal conductivity of 18650 batteries in the range of 3.1 to 3.6 W m^{-1} K^{-1} was obtained by Keil *et al.* through using a thermal impedance spectroscopy and infrared sensors [5].

We have previously reported a phase change material (PCM)-based internal cooling system to alleviate the heat accumulation in 18650 Li-ion batteries [6, 7]. In this work, the internal cooling system we developed is further studied together with the external PCM-based cooling system. A 2D thermal model is first validated on a heating battery equipped with internal or external PCM-based cooling system. It is then used to compare the cooling performance of the internal and external cooling systems on 18650, 21700, and 26650 battery packs of different layers. The battery radial thermal conductivity, PCM thermal conductivity, and exterior convective heat transfer coefficient are adjusted to study their effects on the cooling performance of the internal and external systems. Finally, the advantages and suitable working scenarios of both cooling systems are discussed.

Experiment and Model Setup

Experiment

In this work, a heating battery shown in Fig. 1 was used to experimentally test the cooling performance of the internal and external PCM-based cooling systems, and the obtained temperature data were used to validate the 2D thermal model.

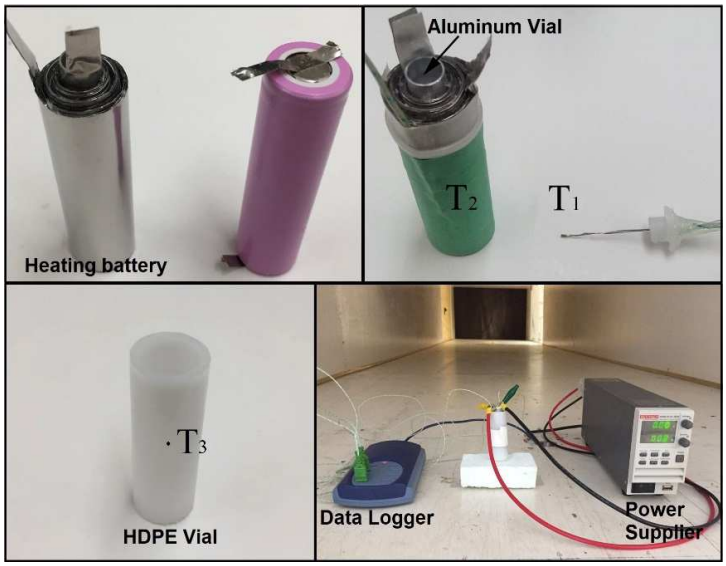

Figure 1. Photographs of the heating battery and the experimental setup.

The heating battery was made by wrapping a stainless steel tape on an aluminum vial. For both tests with the internal and external cooling systems, the heating battery was placed inside a high density polyethylene (HDPE) vial. The internal cooling was achieved by injecting 2.3 ml of PCM into the aluminum vial, while for the external cooling system, the

aluminum vial was left empty and the PCM was injected into the space between the battery and the HDPE vial. The stainless steel tape can be treated as a long resistor because the acrylic adhesive layer on the tape prevent the electrical contact between adjacent layers. The specification and thermal properties of the heating battery are given in Table I.

During the tests, two tabs of the heating battery were connected to a power supplier, and the heating battery was able to generate the heat evenly in its winding similar to the heating process of cylindrical batteries. Temperature at three locations were measured during the experiment, as marked in Fig. 1. The experiment was carried out in a closed wind tunnel to minimize ambient interference.

Table I. Specification and thermal properties of the heating battery.

Parameter	Value	Parameter	Value
Weight (g)	63.6	Inner diameter of HDPE vial (mm)	20.2
Diameter (mm)	19	Outer diameter of HDPE vial (mm)	26
Radial thermal conductivity (W m^{-1} K^{-1})	0.3	Al thermal conductivity (W m^{-1} K^{-1})	201
Averaged specific heat (J kg^{-1} K^{-1})	896	Al specific heat (J kg^{-1} K^{-1})	900
Average density (kg m^{-3})	4596.7	Al density (kg m^{-3})	2700
Inner diameter of Al vial (mm)	7	HDPE thermal conductivity (W m^{-1} K^{-1})	0.45
Outer diameter of Al vial (mm)	7.9	HDPE specific heat (J kg^{-1} K^{-1})	945
Heat generation rate (W m^{-3})	4×10^5	HDPE density (kg m^{-3})	2250

Thermal Model

A 2D thermal model is implemented in this work for simulations. The model is governed by the following energy balance equation:

$$\rho c_p \frac{dT}{dt} = \nabla \cdot (k \nabla T) + q \tag{1}$$

where ρ is the density, c_p is the specific heat, k is the thermal conductivity, T is the temperature, t is the time, and q is the heat generation rate.

Two radial thermal conductivities are used in the thermal model, where one is the measured value of 0.2 W m^{-1} K^{-1} from the literature [2], and the other is calculated based on the following equation:

$$k = \frac{\sum_i l_i}{\sum_i \frac{l_i}{k_i}} \tag{2}$$

where l_i and k_i are the thickness and thermal conductivity of components inside a battery.

In the PCM region, the energy balance equation is same as (1) except without the heat generation term, and the specific heat is calculated as follows:

$$c_p = \begin{cases} c_s & T < T_s \ \text{Solid phase} \\ (1-\gamma)c_s + \gamma c_l + \dfrac{h_f}{T_l - T_s} & T_s < T < T_l \ \text{Solid/liquid phase} \\ c_l & T > T_l \ \text{Liquid phase} \end{cases} \tag{3}$$

where c_s and c_l are the specifics heat of PCM in solid and liquid states, respectively. γ is the PCM liquid fraction, h_f is the latent heat of the PCM, and T_s and T_f are the lower and upper bounds of the melting range of PCM. The physical properties of the PCM (*n*-eicosane) used in this work are summarized in Table II.

Table II. Physical properties of *n*-eicosane [8].

Parameter	Value	Parameter	Value
Solid state specific heat (J kg^{-1} K^{-1})	2150	Solid state density (kg m^{-3})	814
Liquid state specific heat, liquid (J kg^{-1} K^{-1})	2275	Liquid state density (kg m^{-3})	771
Solid state thermal conductivity (W m^{-1} K^{-1})	0.425	Latent heat (kJ kg^{-1})	247.05
Liquid state thermal conductivity (W m^{-1} K^{-1})	0.152	Melting range (°C)	35.7 – 37.1

A convective boundary condition is applied at the exterior surfaces of battery packs, and it can be expressed as:

$$k\frac{\partial T}{\partial y} = h\left(T_{surf} - T_{amb}\right) \quad (4)$$

where h is the convective heat transfer coefficient, T_{surf} and T_{amb} are the cooling surface temperature and ambient temperature, respectively.

Simulation is first carried out on the heating battery for validation and is then used to simulate the temperature of the real cylindrical batteries. Table III summarizes the physical properties of a cylindrical battery used in the thermal model. The heat generation rate was obtained in Ref. [7] on a Samsung ICR18650-26F during a 5 A discharge.

Table III. Physical properties of components used in battery packs.

Parameter	Value	Parameter	Value
Battery diameter (mm)	18.4, 21, 26	Can specific heat (J kg^{-1} K^{-1})	502
Mandrel diameter (mm)	2.5	Can density (kg m^{-3})	7861
Can thickness (mm)	0.3	Cell specific heat (J kg^{-1} K^{-1})	830 [9]
Can thermal conductivity (W m^{-1} K^{-1})	16.3	Cell density (kg m^{-3})	2580 [9]
Cell thermal conductivity (W m^{-1} K^{-1})	1.97, 0.2	Foam specific heat (J kg^{-1} K^{-1})	1300
Foam thermal conductivity (W m^{-1} K^{-1})	0.032	Foam density (kg m^{-3})	40
Heat generation rate (W m^{-3})	59235		

Results and Discussion

Model Validation

During the test, the HDPE vial was heated to 50°C and cooled to room temperature to obtain the convective heating transfer coefficient at its surface. After matching with the simulation result, a convective heat transfer coefficient of 20 W m^{-2} K^{-1} was obtained and applied at the surface of HDPE vial as the boundary condition. The experimental and simulation results are summarized in Fig. 2. It is seen that the temperature at the surface (T_2) of the heating battery equipped with the internal and external cooling systems are very close, with a value of around 48.8°C, while the temperature inside the heating battery that equipped with the internal PCM cooling system is much lower than that equipped with the external cooling system. The recorded temperature differences inside the heating battery ($T_1 – T_2$) are 4.1°C and 9.3°C in the internal and external cooling systems, respectively.

Simulation results of the 2D thermal model are plotted in Fig. 2 in solid curves. It is seen that for both the internally and externally cooled battery, the simulated temperatures at the assigned three locations agree well with the experimental results. The validated 2D thermal model is then used to simulate the thermal responses of battery packs in the following sections.

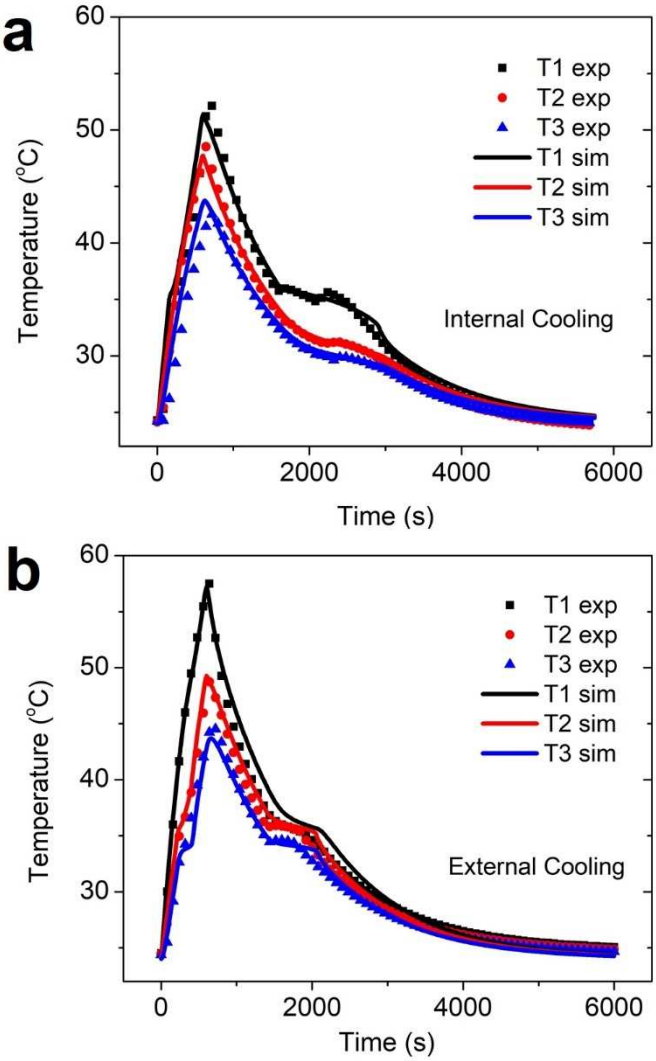

Figure 2. Comparison of the experimental and simulated temperature profiles of the heating battery equipped with a) internal PCM-based cooling system and b) external PCM-based cooling system.

Battery Pack Simulations

Battery packs with 2, 4, and 8 layers of batteries are created in the model for simulation. For each battery pack, three battery sizes are studied, with diameters of 18.4 mm, 21 mm, and 26 mm. Meanwhile, the battery radial thermal conductivity and PCM thermal conductivity are set to variables during the simulations to investigate their effects on the thermal responses of batteries.

For all simulations, the pass criteria of a cooling system are that the system can maintain the maximum temperature and temperature difference of the jelly rolls below 50°C and 5°C, respectively. For the internal PCM cooling system, the PCM radius is set to 3.8 mm [7], 4.38 mm, and 5.4 mm for 18650, 21700, and 26650 batteries, respectively. While in the external PCM cooling system, the PCM is placed in the void spaces between batteries, where the distances between batteries are adjusted to ensure the ratio of PCM amount to battery winding amount is the same as the internal cooling system. All simulations are started with using the calculated battery radial thermal conductivity (1.97 W m^{-1} K^{-1}) and the pure PCM thermal conductivity given in Table I, named as Case 1. In Case 2, the battery radial thermal conductivity is reduced to 0.2 W m^{-1} K^{-1} to study if the cooling systems can meet the pass criteria on batteries with a low radial thermal conductivity. In Case 3, the thermal conductivity of PCM is increased to 10 W m^{-1} K^{-1} to offset the temperature increase caused by the reduced radial thermal conductivity of batteries. Case 4 is applied when the cooling systems in Case 1 cannot meet the pass criteria, and the thermal conductivity of the batteries and PCM are 1.97 W m^{-1} K^{-1} and 10 W m^{-1} K^{-1}, respectively.

Fig. 3 shows the temperature and temperature difference of the 2-layer battery pack at the end of the 5 A discharge in a perfectly thermally insulated environment (h = 0 W m^{-2} K^{-1}). The black or grey columns are the results of internally cooled battery packs, and the red and blue columns are that of the externally cooled battery packs. It can be seen that as the batteries become thicker, the temperature and temperature difference increase in both internal and external PCM cooling systems.

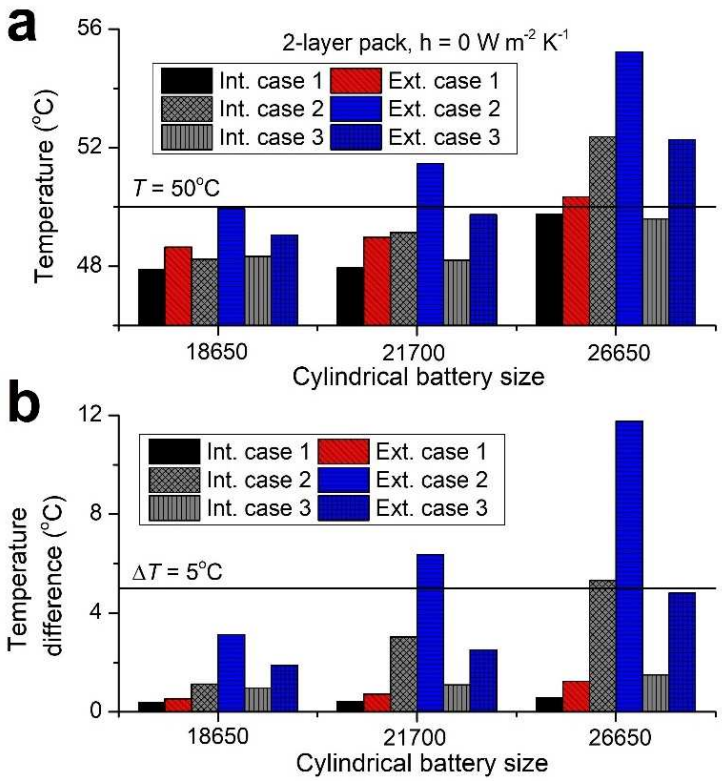

Figure 3. a) Temperature and b) temperature difference of the 2-layer battery pack at the end of 5 A discharges in a perfectly thermally insulated environment (h = 0 W m^{-2} K^{-1}).

For Case 1, all of the batteries meet the pass criteria except the 26650 battery pack with the external PCM cooling system, which has a maximum temperature above 50°C. As the radial thermal conductivity drops to 0.2 W m^{-1} K^{-1} (Case 2), both battery packs with internal and external cooling systems experience increases in their temperature and temperature difference. And bigger temperature increases are found in the external PCM cooling systems, which indicates the external system is not as effective as the internal system in dealing with battery packs with low radial thermal conductivities. In Case 2, both the 21700 and 26650 battery packs with the external system and the 26650 battery with the internal system are failed to meet the pass criteria. To address the issue, the PCM thermal conductivity is increased to 10 W m^{-1} K^{-1} (Case 3). It is seen that a high thermally conductive PCM can, to an extent, offset the reduced thermal conductivity of batteries, and bigger temperature drops are found in the battery packs with the external PCM system.

Fig.4 shows the cooling results of the 2-layer 21700 battery pack with internal and external PCM systems in different convective cooling conditions. The cooling boundary condition of the battery pack is shown in Fig. 5, where convection cooling is applied on top and bottom surfaces of the pack and insulation is applied on left and right side of the computation unit. The batteries in the external PCM system are 0.4 mm apart from each other in the horizontal direction. In Fig. 4a, it is seen that the maximum temperature drops as the heat transfer coefficient increases, but the temperature difference in the battery pack increases significantly, as shown in Fig. 4b. For all simulations, the internal PCM system outperforms the external system except the Case 1 simulation in a forced convection condition (h = 100 W m^{-2} K^{-1}). This is because the PCM in the external cooling system is more effective in distributing the heat, while the direct contact between batteries and aluminum wall in the internal cooling design creates a cold spot at the contact region and leads to a bigger temperature difference, as shown in Fig. 5.

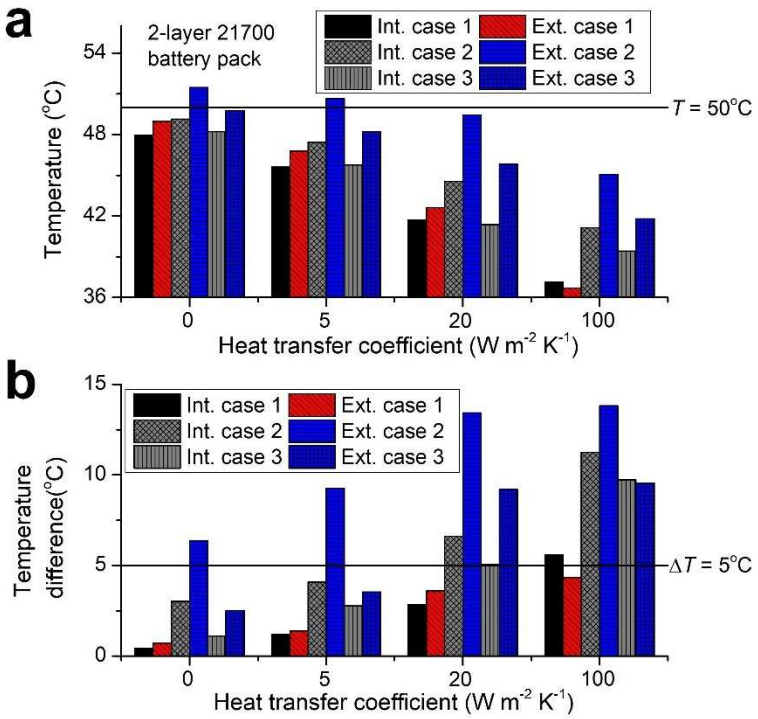

Figure 4. a) Temperature and b) temperature difference of the 2-layer 21700 battery pack at the end of 5 A discharges in different convective cooling conditions.

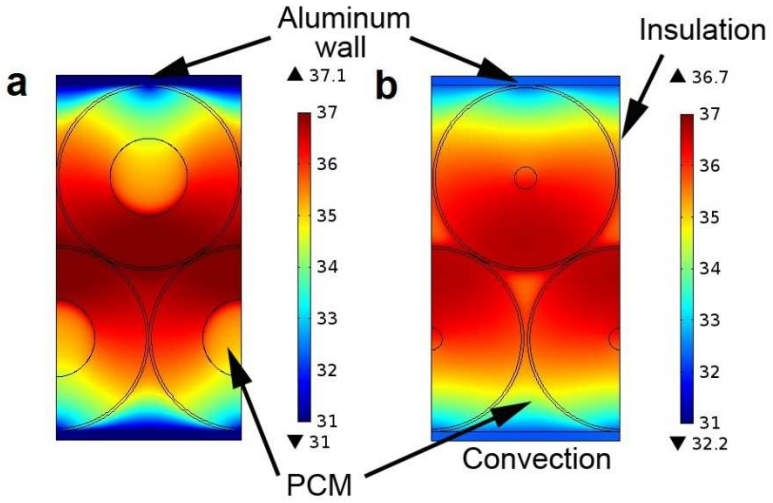

Figure 5. Temperature contours of the a) internally and b) externally PCM cooled 21700 battery packs at the end of 5 A discharges.

In Fig. 6, the temperature and temperature differences of the 18650 battery pack are plotted against the layer number at h = 0 W m^{-2} K^{-1}. It is seen that the temperature and temperature difference of the internally cooled battery pack increases slightly with the increases of the layer number, while they increase significantly in the externally cooled battery pack. It is noteworthy that the external PCM cooling system shows difficulty in managing the heat generation of batteries with a low radial thermal conductivity, especially for large-size battery packs. In comparison, the internal PCM cooling system shows strength in dealing with large battery packs.

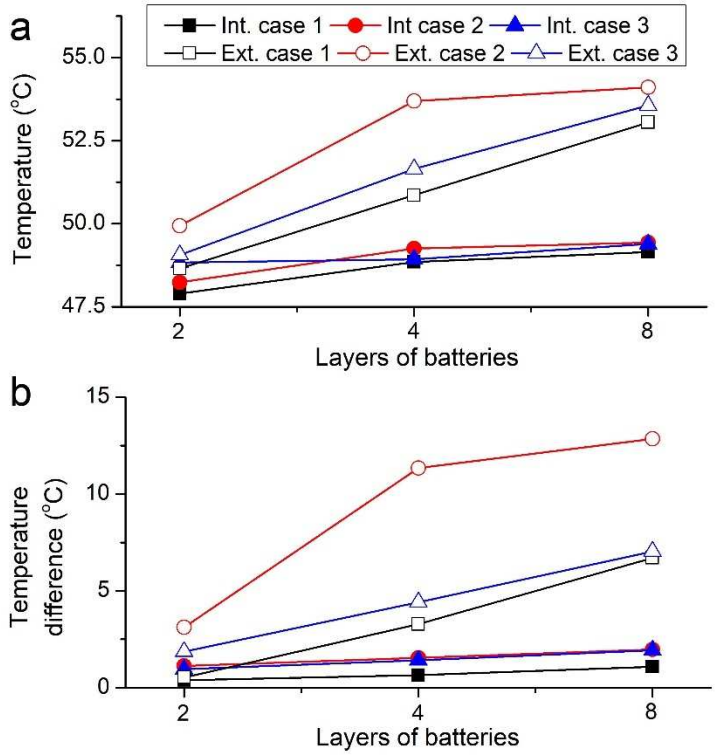

Figure 6. Plots of a) temperature and b) temperature difference of 18650 battery packs versus battery layer number in a perfectly insulated environment (h = 0 W m^{-2} K^{-1}).

The simulation results of the 4-layer 21700 battery pack in different convective cooling conditions are shown in Fig. 7. With the increase of the battery layer number, the external cooling system is unable to meet the both the temperature and temperature difference pass criteria except Case 4 in natural convection or insulated conditions, which suggests that a high thermally conductive PCM is very necessary for the external PCM cooling system. Meanwhile, for the 4-layer battery pack, the drops in the peak temperature with the increase of heat transfer coefficient at the pack walls are not as notable as the 2-layer battery pack.

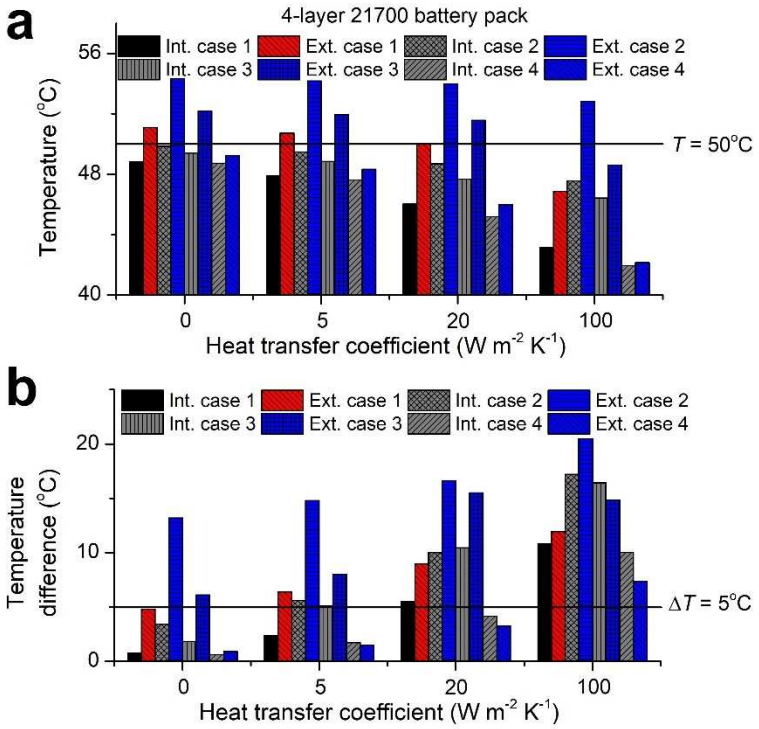

Figure 7. a) Temperature and b) temperature difference of the 4-layer 21700 battery pack at the end of 5 A discharges in different convective cooling conditions.

Fig. 8 shows the results of the 8-layer 21700 battery packs in different convection conditions. It is found that in most cases (Case 1, 2, and 3), the increase of the convective heat transfer coefficient at the battery pack surfaces is not helpful in reducing the peak temperatures inside the 8-layer battery packs, which is attributed the fact that the low thermal conductivity of either battery or PCM as well as the long heat transfer distance hinder the effective heat exchange between the battery pack center and its surfaces. In Fig. 8b, the temperature differences of 8 layers of batteries are shown. It is seen that as the heat transfer coefficient increases to and above 20 W m^{-2} K^{-1}, the temperature differences in all simulation cases exceed the required 5°C. Therefore, cooling at the battery pack side walls should be avoided for large-size battery packs. Meanwhile, it is found that using high thermally conductive PCM in the 8-layer battery pack can only slightly improve the temperature uniformity.

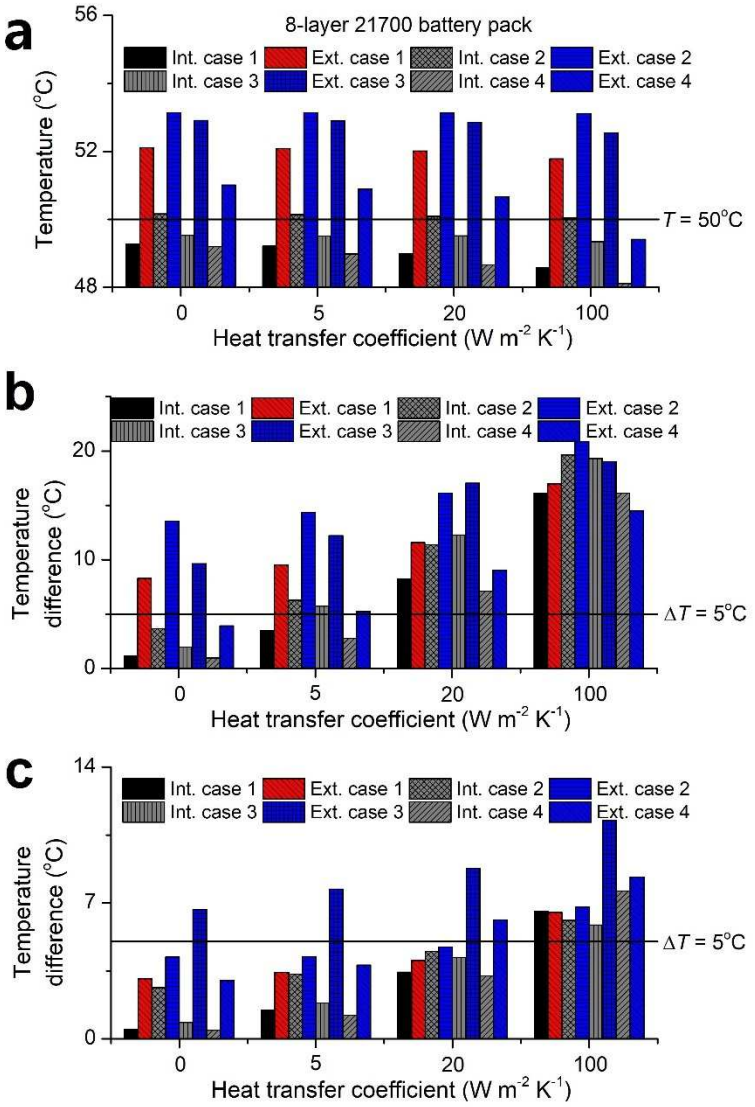

Figure 8. a) Temperature and b) 8-layer and c) 6-layer temperature differences of the 8-layer 21700 battery pack at the end of the 5 A discharge in different convective cooling conditions.

The temperature contour of the internally cooled battery pack under forced convection condition (h = 100 W m^{-2} K^{-1}) is shown in Fig. 9a, it is seen that the temperature drop occurs mainly on the outmost battery layer. To address this issue, side wall insulation can be considered on large battery packs. As an example, a 2 mm PS foam and 3 mm PC layers are installed in between the aluminum walls and the outmost battery layers. As seen in Fig. 9b, with the insulation layers, the temperature uniformity of the battery pack is highly improved, and a temperature difference of 3.4°C is achieved at the end of discharge in a forced convection condition (h = 100 W m^{-2} K^{-1}). Bottom convective cooling can be considered to enhance the thermal performance of the system without sacrificing the temperature uniformity. As shown in Fig. 9c and d, when a convection boundary condition of using h = 20 and 100 W m^{-2} K^{-1} is applied at the bottom surface of the battery pack, lower battery temperatures can be obtained, and the temperature differences are maintained below 3°C. The side wall heat transfer coefficient used in the model is 20 W m^{-2} K^{-1}.

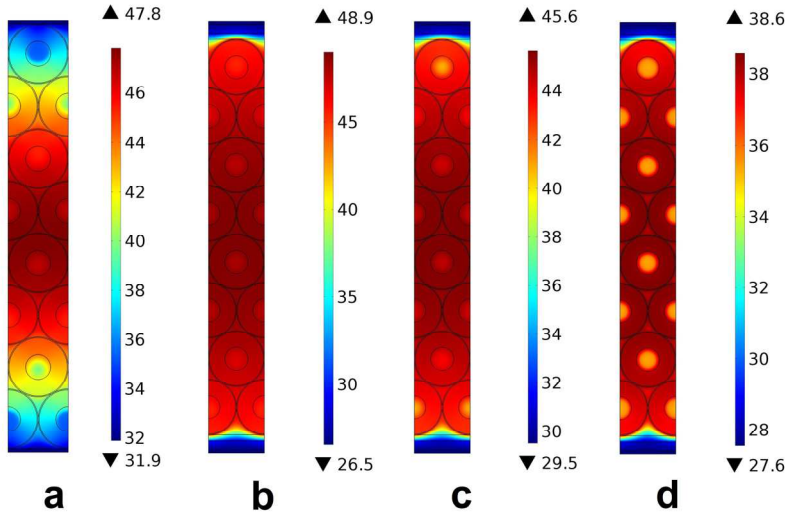

Figure 9. Temperature contours of the 8-layer 18650 battery pack equipped with the internal PCM cooling system, a) battery pack with aluminum pack walls (h = 100 W m^{-2} K^{-1} at pack walls), b) battery pack with PS foam insulation (h = 100 W m^{-2} K^{-1} at pack walls), c) bottom cooled battery pack with PS foam insulation (h = 20 W m^{-2} K^{-1} at both pack walls and bottom), d) bottom cooled battery pack with PS foam insulation (h = 20 W m^{-2} K^{-1} at pack walls, h = 100 W m^{-2} K^{-1} at pack bottom).

Overall, when using a limited amount of PCM to maintain the battery temperature within the preset range, the internal PCM cooling system is more suitable for large battery packs than the external PCM cooling system due to the lower peak temperature and better temperature uniformity. The external PCM cooling system can be considered for thinner battery packs with a forced convective cooling on the side walls, and a high thermal conductivity of both PCM and battery is required. One advantage of the external cooling system is that it can fully utilize the void spaces between cylindrical batteries. Fig. 10 shows the repeating unit in a cylindrical battery pack, where the void ratio is 10.27%. If a high energy density is a necessity of an application, the external cooling system may be used and further modified to meet the requirement, or the internal cooling system can be combined with the external system to fully utilize the void spaces. If a high specific energy is required for an application, the internally cooled batteries can be directly used to assemble battery packs.

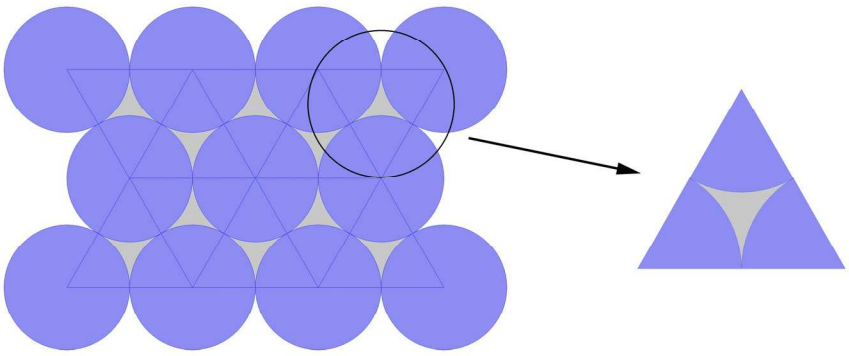

Figure 10. An illustration of a cylindrical battery pack and its repeating unit used for void ratio calculation.

Conclusion

In this work, the internal and external-based PCM cooling systems are thoroughly compared in their performance and suitability for the thermal management of cylindrical batteries in high rate discharges. The battery size, battery layer number, battery radial thermal conductivity, and PCM thermal conductivity are used as variables in the thermal model to investigate their effects on the performance of the internal and external cooling systems. The internal cooling system outperforms the external system for most of the simulations, while the external cooling system is more suitable for a 2-layer battery pack with forced convection applied at the battery pack side walls. The increases of the battery size and layer number, or the decreases of the battery and PCM thermal conductivity all can lead to a higher temperature and temperature difference inside the battery packs. And results showed that the externally cooled battery packs are more sensitive to these changes than the internally cooled battery packs. For large size battery packs, convection cooling at the side walls of battery packs can lead to temperature nonuniformity and should be avoided, while convection cooling at the bottom or top battery pack surface is helpful in reducing the peak temperature while ensuring a uniform temperature distribution.

Acknowledgement

The authors sincerely thank the postdoctoral fellowship from the National Sciences and Engineering Research Council of Canada (NSERC).

References

1. R. Zhao, S. Zhang, J. Liu, and J. Gu, *J. Power Sources*, **299**, 557-577 (2015).
2. K. Shah, C. Mckee, D. Chalise, and A. Jain, *Energy*, **113**, 852-860 (2016).
3. G. Zhang, L. Cao, S. Ge, C. Y. Wang, C. E., Shaffer, and C. D. Rahn, *J. Electrochem. Soc.*, **161**, 1499-1507 (2014).
4. H. Bhundiya, M. Hunt, and B. Drolen, *Thermal and Fluids Analysis Workshop*, Houston, TX (2018).
5. P. Keil, K. Rumpf, and A. Jossen, *World Electr. Veh. J.*, **6**, 581-591 (2013).
6. R. Zhao, J. Gu, and J. Liu, *Int. J. Energy. Res.*, **42**, 2728-2740 (2018).
7. R. Zhao, J. Gu, and J. Liu, *Energy*, **135**, 811-822 (2017).
8. C. Vélez, M. Khayet, and J. M. Ortiz de Zárate, *Appl. Energy,* **143**, 383-394 (2015).
9. T. D. Hatchard, D. D. MacNeil, A. Basu, and J. R., Dahn, *J. Electrochem. Soc*., **148**, A755-A761 (2001).